Title

Does hydrologic circulation mask frictional heat on faults after large earthquakes?

Journal

Journal of Geophysical Research, 115(B9)

Authors

Fulton, Patrick M.
Harris, Robert N.
Saffer, Demian M.
et al.

Publication Date

2010-09-03

Peer reviewed

Does hydrologic circulation mask frictional heat on faults after large earthquakes?

Patrick M. Fulton,[1] Robert N. Harris,[1] Demian M. Saffer,[2] and Emily E. Brodsky[3]

Received 2 November 2009; revised 17 March 2010; accepted 30 April 2010; published 3 September 2010.

[1] Knowledge of frictional resistance along faults is important for understanding the mechanics of earthquakes and faulting. The clearest in situ measure of fault friction potentially comes from temperature measurements in boreholes crossing fault zones within a few years of rupture. However, large temperature signals from frictional heating on faults have not been observed. Unambiguously interpreting the coseismic frictional resistance from small thermal perturbations observed in borehole temperature profiles requires assessing the impact of other potentially confounding thermal processes. We address several issues associated with quantifying the temperature signal of frictional heating including transient fluid flow associated with the earthquake, thermal disturbance caused by borehole drilling, and heterogeneous thermal physical rock properties. Transient fluid flow is investigated using a two-dimensional coupled fluid flow and heat transport model to evaluate the temperature field following an earthquake. Simulations for a range of realistic permeability, frictional heating, and pore pressure scenarios show that high permeabilities ($>10^{-14}$ m^2) are necessary for significant advection within the several years after an earthquake and suggest that transient fluid flow is unlikely to mask frictional heat anomalies. We illustrate how disturbances from circulating fluids during drilling diffuse quickly leaving a robust signature of frictional heating. Finally, we discuss the utility of repeated borehole temperature profiles for discriminating between different interpretations of thermal perturbations. Our results suggest that temperature anomalies from even low friction should be detectable at depths >1 km 1 to 2 years after a large earthquake and that interpretations of low friction from existing data are likely robust.

Citation: Fulton, P. M., R. N. Harris, D. M. Saffer, and E. E. Brodsky (2010), Does hydrologic circulation mask frictional heat on faults after large earthquakes?, *J. Geophys. Res.*, *115*, B09402, doi:10.1029/2009JB007103.

1. Introduction

[2] Frictional resistance along faults is an important parameter controlling earthquake nucleation and propagation. Because friction is central to earthquake mechanics, considerable effort has gone into characterizing fault zone friction both in the laboratory and in situ [e.g., *Scholz*, 2002]. Laboratory measurements suggest that the intrinsic low-speed friction coefficient for most rocks is approximately 0.60−0.85 [*Byerlee*, 1978]. This magnitude of friction is hypothesized to generate large thermal anomalies on natural faults with large slip rates and/or large total displacements, assuming hydrostatic pore pressure. Curiously, analysis of surface heat flow data [e.g., *Brune et al.*, 1969; *Lachenbruch and Sass*, 1980; *Wang et al.*, 1995] and subsurface temperature profiles [*Yamano and Goto*, 2001; *Kano et al.*, 2006; *Tanaka et al.*, 2006, 2007] that cross fault zones do not show substantial, unequivocal anomalies from frictional heating. These observations prompt two questions: (1) could the frictional resistance be as large as expected from Byerlee's law and hydrostatic pore pressure, but the heat signal is masked or dissipated by other processes? (2) If not, what is the in situ value of frictional resistance during fault slip?

[3] Much effort has been spent recently on the second of these questions resulting in theoretical models supported by both laboratory and field observations that suggest that coseismic friction may be quite low [e.g., *Brodsky and Kanamori*, 2001; *Di Toro et al.*, 2004; *Rice*, 2006; *Ma et al.*, 2006], but considerably, less work has been conducted on the first question. Studies of processes that may mask or dissipate the frictional heat signal have focused on steady state topographically driven or buoyancy-driven groundwater flow [*Williams and Narisimhan*, 1989; *Saffer et al.*, 2003; *Fulton et al.*, 2004] and the effects of heterogeneous thermal properties [*Tanaka et al.*, 2007; *Fulton and Saffer*, 2009a]. One candidate for obscuring a frictionally generated thermal signal that has not been fully explored is transient groundwater flow following an earthquake [e.g., *Kano et al.*, 2006; *Scholz*, 2006].

[1] College of Oceanic and Atmospheric Sciences, Oregon State University, Corvallis, Oregon, USA.
[2] Department of Geosciences, Pennsylvania State University, University Park, Pennsylvania, USA.
[3] Department of Earth and Planetary Sciences, University of California, Santa Cruz, California, USA.

0148-0227/10/2009JB007103

Table 1. Definition of Symbols

Symbol	Parameter	Units (Dimensions)
C	specific heat capacity	J kg^{-1} $°C^{-1}$ (L^2 T^{-1} t^{-2})
d	fault displacement	m (L)
g	gravitational acceleration	m s^{-2} (Lt^{-2})
H	average rate of frictional heat generation per unit area	W m^{-2} (Mt^{-3})
P	pore fluid pressure	Pa ($ML^{-1}t^{-2}$)
T	Temperature anomaly	°C (T)
t	time	s (t)
v	slip velocity	m s^{-1} (Lt^{-1})
y	distance from fault zone	m (L)
z	Depth	m (L)
α	thermal diffusivity	m^2s^{-1} (L^2t^{-1})
λ	pore pressure ratio: P/σ_v	dimensionless
μ	fault zone friction coefficient	dimensionless
μ_c	country rock friction coefficient	dimensionless
ρ	bulk rock density	kg m^{-3} (ML^{-3})
σ_n	total normal stress	Pa (ML^{-1} t^{-2})
σ_n'	effective normal stress: $\sigma_n - P$	Pa (ML^{-1} t^{-2})
σ_v	total overburden stress: ρgz	Pa (ML^{-1} t^{-2})

[4] We first explore the potential effects of transient groundwater flow on the dissipation and redistribution of frictionally generated heat. Because our attention is on frictional heat generation during an earthquake and transient groundwater flow within the few years after an earthquake, we focus our study on the effects of these processes in the near field where they are most likely discernable. Our evaluation of the potential effects of transient groundwater flow on fault zone temperature anomalies is driven by three specific questions: (1) how big is the expected temperature anomaly from frictional heating as a function of time?, (2) what permeability values are required to yield significant advective disturbances?, and (3) how does advection affect frictional heat anomalies for different fault zone permeability architectures (i.e., are fault conduits or barriers to fluid flow)? Understanding the answers to these questions is important for designing experiments to detect frictional heating and for unambiguously interpreting thermal data in terms of frictional heat generation and resistance during slip.

[5] In the following sections, we address these questions and discuss the implications of their answers. After reviewing the relationship between earthquake slip, stress and friction, and frictional heat generation (section 2), we present numerical models of coupled fluid flow and heat transport and evaluate the role of transient fluid flow in affecting a frictional heat signal for a range of realistic hydrogeologic and frictional heating scenarios (sections 3 and 4). We then evaluate other processes associated with borehole temperature measurements that may mask or dissipate the frictional heating signal and present strategies for overcoming some of these obstacles that might improve our ability to detect and unambiguously interpret frictional heating (section 5). The implications of these results for interpretations of the frictional resistance along faults during earthquake slip from previous borehole experiments are also discussed (section 6).

2. Frictional Heat Generation and Thermal Perturbations

[6] The conductive temperature anomaly T across a fault due to frictional heating can be expressed by the equation for one-dimensional diffusion of a plane source of heat [*Carslaw and Jaeger*, 1959],

$$T(y,z,t) = \left(\frac{\mu\sigma_n'(z)d}{c\rho}\right)\left(\frac{e^{-y^2/4\alpha t}}{2\sqrt{\pi\alpha t}}\right). \quad (1)$$

The first term of equation 1 describes the frictional heating source strength (in units of °C-m) showing the functional dependence on fault displacement d; the specific heat and density of the surrounding rock c and ρ, respectively; and the frictional resistance (i.e., shear stress) on the fault, defined by the product of the displacement-averaged fault zone friction coefficient during slip μ, and effective normal stress, $\sigma_n'(z)$, which is a function of depth z and pore pressure. Symbols and their units are defined in Table 1. The second term describes the diffusion of heat as a function of distance from the fault plane y, time t, and the thermal diffusivity α. For an optimally oriented thrust fault, the effective normal stress can be described by

$$\sigma_n'(z) = \frac{(1-\lambda)\sigma_v}{(1+\mu_c{}^2) - \mu_c\sqrt{1+\mu_c{}^2}} \quad (2)$$

[*Lachenbruch and McGarr*, 1990], where μ_c is the intrinsic friction coefficient of the surrounding rock and λ is the pore pressure ratio defined as P/σ_v, where P is the pore pressure and σ_v is the total overburden stress, defined as ρgz, where g is gravity. Evaluating the frictional heat generation for a thrust fault allows us to compare our results with measurements acquired across the Chelungpu fault after a large thrust earthquake [*Kano et al.*, 2006; *Tanaka et al.*, 2006].

[7] Equations 1 and 2 show that, in general, the temperature perturbation scales with the product of μ and σ_n' and attenuates with the product of thermal diffusivity and time. These relationships are shown graphically in Figure 1 for a fault at depths of 1 and 2 km and with an average coefficient of friction during slip of 0.1 and 0.6. The area under the curves is proportional to the total frictional heat. If λ does not vary significantly with depth, the effective normal stress increases with depth leading to an increased frictional heat signal. The low rates of frictional heating interpreted from existing thermal data could result from a low friction coefficient on the fault, elevated pore pressure, or a combination of the two [e.g., *Lachenbruch and Sass*, 1980; *Rice*, 1992; *Fulton and Saffer*, 2009]. In addition, elevated pore pressure that weakens the fault could be sustained throughout the seismic cycle or transiently generated during rapid slip [e.g., *Rice*, 1992; *Segall and Rice*, 2006; *Andrews*, 2002]. For simplicity, we represent different fault strength (frictional resistance) scenarios in terms of the equivalent friction coefficient assuming hydrostatic pore pressure, defined as the product of the friction coefficient during slip and effective normal stress divided by effective normal stress assuming hydrostatic pore pressure.

3. Coupled Heat and Fluid Flow Models

[8] We evaluate the role of transient groundwater flow on fault zone temperature following an earthquake using 2-D finite element models to solve the coupled equations of transient fluid flow and heat transport with the algorithm SUTRA [*Voss*, 1984]. The governing equations, based on the

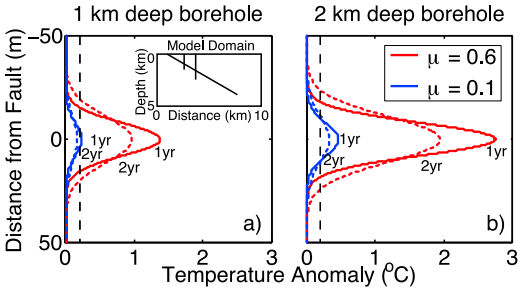

Figure 1. Frictional temperature anomalies in the absence of fluid circulation resulting from a thrust earthquake with 5 m of slip on a fault with 30° dip and assuming a thermal diffusivity of 10^{-6} m^2 s^{-1}. The separate curves illustrate how a temperature anomaly from frictional heating evolves as a function of time and depth for both large and small coefficients of friction during slip assuming hydrostatic pore pressure. (a) Temperature anomalies for a borehole intersecting the fault at a depth of 1 km. The vertical axis represents the perpendicular distance from the fault zone. Red and blue lines correspond to friction coefficients of 0.6 and 0.1, respectively, assuming hydrostatic pore pressure. Solid and dashed lines show the frictional heating anomaly 1 and 2 years after the earthquake, respectively. The dashed vertical black line shows a conservative detection threshold of 0.2°C. (b) Temperature anomaly for a borehole intersecting the fault at a depth of 2 km.

conservation of energy and mass, are listed in Appendix A and described in detail in the study by *Voss* [1984]. The model domain is based on the geologic cross section of *Yue et al.* [2005] for the Chelungpu fault in the area near the Taiwan Chelungpu-fault Drilling Project boreholes, in which temperature was measured across the Chelungpu fault after the 1999 M_w 7.6 Chi-Chi earthquake [*Kano et al.*, 2006; *Tanaka et al.*, 2006]. Boundary conditions and material properties are based on thermal data from the same area [*Tanaka et al.*, 2007]. The model domain is 10 km wide and 5 km deep (Figure 1, inset) and contains a thrust fault with a surface trace 1 km from the left side of the model that dips to the right at 30°. The fault extends to a depth of 4 km. The model consists of 31,896 quadrilateral elements that are each 1 m thick and cover areas ~3×10^0 to ~2.5×10^5 m^2, with the highest resolution near the fault.

[9] We set the surface boundary condition at atmospheric pressure and mean annual surface temperature, 101,325 Pa and 21.6°C. We prescribe a heat flux of 37 mW/m^2 across the basal boundary and assign a constant radioactive heat production of 1.6 μW/m^3, resulting in a steady state surface heat flow of ~45 mW/m^2 [*Tanaka et al.*, 2007]. There are no internal fluid sources, and the side boundaries are closed to both fluid flow and heat transfer. Parameter values for material properties are given in Table 2.

[10] We initialize temperatures for our transient simulations by running steady state simulations with no frictional heating on the fault. In our transient simulations, frictional heat generation on the fault is prescribed for a slip duration of 2 s. The assumed slip velocity of 2.5 m/s results in a total slip of 5 m, a reasonable value for M_w ~7 earthquakes and a value representative of estimates for the M_w 7.6 Chi-Chi earthquake [*Ma et al.*, 2001]. The average rate of frictional heat generation per unit area H is given by

$$H(z) = \mu\sigma_n'(z)v, \tag{3}$$

where v is the slip velocity, and $\sigma_n'(z)$ is the effective normal stress defined by equation 2. We consider two cases for frictional heat generation: a "weak fault" scenario in which frictional resistance on the fault increases by 2.4 MPa/km depth, consistent with hydrostatic pore pressure and a fault zone friction coefficient during slip of $\mu = 0.1$, and a "strong fault" scenario in which frictional resistance increases by 14.2 MPa/km, as expected for hydrostatic pore pressure and a friction coefficient of 0.6. These cases correspond to frictional heat generation on the fault that increases from zero at the surface by 5.9 or 35.6 W/m^2/km depth, respectively. A value of $\mu = 0.1$ for our weak fault scenario corresponds to the values of friction assuming hydrostatic pore pressure interpreted from temperature observations across the Chelungpu fault [*Tanaka et al.*, 2006; *Kano et al*, 2006], from stress orientations inferred from earthquake focal mechanisms near the San Andreas fault [e.g., *Townend and Zoback*, 2004] and from observations made during high-speed friction tests [e.g., *Tanikawa and Shimamoto*, 2009].

[11] Model simulations start with two 1 s time steps corresponding to the period of frictional heating. To evaluate the potential effects of advection by fluid flow, we assume pore pressure increases from hydrostatic to lithostatic within the fault zone and to 80% of lithostatic in the country rock immediately after the earthquake. By incorporating a large pore fluid pressure gradient to drive fluid flow, these simulations produce the largest likely advective disturbance to the thermal field for each permeability scenario we evaluate.

Table 2. Parameter Values Used in Simulations

Parameter	Value	Reference
Porosity	0.10	*Tanaka et al.* [2007]
Bulk thermal conductivity	2.5 W m^{-1} K^{-1}	
Thermal conductivity, fluid	0.6 W m^{-1} K^{-1}	*Voss* [1984]
Thermal conductivity, matrix	2.582 W m^{-1} K^{-1}	
Specific heat capacity, fluid	4182 W kg^{-1} K^{-1}	*Voss* [1984]
Specific heat capacity, matrix	840 W kg^{-1} K^{-1}	*Tanaka et al.* [2007]
Density, matrix	2600 kg m^{-3}	
Density, fluid at 20°C	1000 kg m^{-3}	*Voss* [1984]
Coefficient of fluid density change	$^{-}$0.375 kg m^{-3} K^{-1}	*Voss* [1984]
Bulk thermal diffusivity	1×10^{-6} m^2 s^{-1}	*Voss* [1984]
Compressibility, matrix	4×10^{-10} Pa^{-1}	*Voss* [1984], *Neuzil* [1986], *Ge and Garven* [1992]
Compressibility, fluid	1×10^{-9} Pa^{-1}	*Voss* [1984]

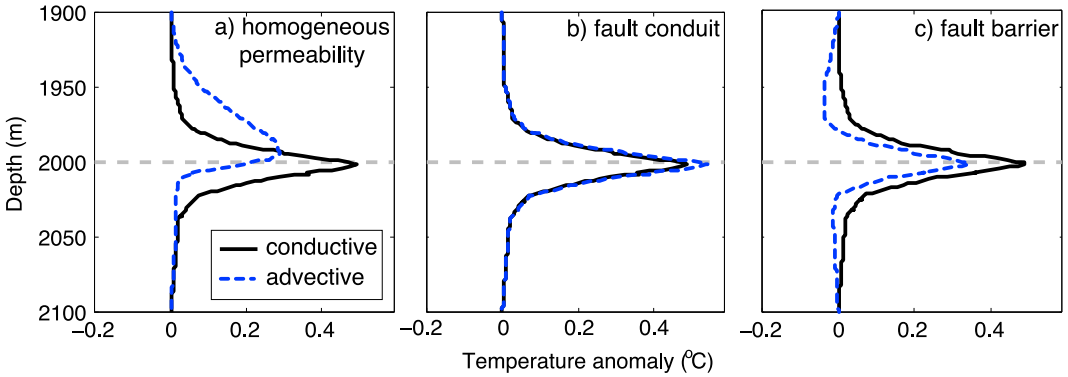

Figure 2. Frictional heating anomalies from model simulations with transient fluid flow (blue lines) and without (black lines), 2 years after an earthquake. Note that the vertical axis is more compressed than in Figure 1 and represents the depth along vertical profiles that cross a dipping fault zone at 2 km. Conductive anomalies correspond to low-frictional heating scenarios with a friction coefficient during slip of 0.1, 5 m of fault slip, and a fault intersection depth of 2 km. The advective scenarios have permeability values of 10^{-14} m^2 for (a) the entire model domain, (b) within a 10 m wide fault zone corresponding to a fault conduit, and (c) only within the country rock surrounding a 10 m low-permeability fault zone acting as a fault barrier.

The pore fluid gradients are then allowed to dissipate, and the model simulations are evaluated 32 s after faulting and then at time steps that progressively increase in duration by 2 orders of magnitude until they reach a period of roughly 1 year, after which the subsequent time steps are held constant at 1 year durations. Models are evaluated for a range of realistic permeability values and fault zone architectures, described in section 4.

4. Modeling Results: Thermal Effects of Transient Fluid Flow

[12] We first consider a scenario in which permeability is uniform for the fault zone and country rock. We evaluate heat transport for permeabilities ranging from 10^{-14}–10^{-19} m^2. This range of permeabilities is consistent with bulk crustal permeability estimates of ~10^{-17}–10^{-16} m^2 determined from deep drilling [e.g., *Townend and Zoback*, 2000] and values of fracture permeability within zones that host seismicity due to reservoir impoundment estimated to generally range from 5×10^{-16} to 5×10^{-14} m^2 [*Talwani et al.*, 2007]. For our simulations, high permeabilities (≥10^{-14} m^2) are needed for transient groundwater flow to significantly affect temperatures across the fault within a few years after an earthquake. Although a permeability of 10^{-14} m^2 is somewhat high for country rock, it is within the range of reported values for fault breccia [e.g., *Mizoguchi et al.*, 2008]. Over time fluids move upward driven by both the diffusion of the initial fluid pressure field prescribed immediately after the earthquake and by thermal buoyancy. For simulations with uniform permeability of 10^{-14} m^2, the vertical fluid flow rate immediately after the earthquake is ~8×10^{-5} m s^{-1} at 2 km depth and diminishes to ~4×10^{-6} m s^{-1} within the first year. Horizontal fluid flow rates near the fault are 10%–50% of the vertical fluid flow rate over this time period. The fluid flow in the most permeable scenario acts to spread out the frictional heat anomaly. This effect decreases the peak temperature anomaly, displaces the anomaly upward, and increases its asymmetry relative to the conductive case (Figure 2a). Because the maximum temperature anomaly provides a reasonable measure of the ability to resolve a frictional heat signal, it is useful to consider its attenuation as a function of time relative to the conductive case (Figure 3). For a uniform permeability of 10^{-14} m^2, advection diminishes the frictional heat anomaly by ~30% after 1 year and ~50% after 6 years relative to the conductive case (Figure 3b).

[13] In a second set of simulations, we evaluate the effect of a fault zone conduit consisting of a 10 m wide high permeability zone within lower permeability country rock. We consider fault zone permeabilities from 10^{-14} to 10^{-18} m^2 with the country rock permeability held at 10^{-19} m^2. We find that fault zone permeabilities of ~10^{-14} m^2 are required for fluid flow to cause significant deviation from the conductive solution. Fluid flow rates are comparable to the previous scenario but are controlled by the permeability structure. In this scenario, the frictional heat signal at the fault is increased slightly as fluids advect heat from depth along the fault zone, driven both by the elevated pore pressure assigned in the fault zone and by thermal buoyancy (Figure 2b). This effect is less than 0.1°C. In our low-friction case, the disturbance constitutes a significant fraction of the total anomaly, roughly 6% above the conductive solution 1 year after the earthquake and ~40% after 6 years for our highest permeability scenario (Figure 3b). Increasing the width of the fault conduit up to 200 m increases the advective temperature anomaly, but for fault zone thicknesses beyond 200 m, the effect becomes similar to the homogenous high permeability scenario described above. Some earthquake sequences have been interpreted to be driven by the rapid migration of high-pressured fluids and have been modeled to occur within fault zones with transient permeability values as large as 10^{-11} m^2 [*Noir et al.*, 1997; *Miller et al.*, 2004]. If permeability is truly this high following an earthquake, our model results suggest that a large increase in temperature within the fault zone would ensue due to updip migration of warm fluids. The lack of large observed temperature anomalies across fault zones [*Yamano and Goto*, 2001; *Tanaka et al.*, 2006; *Kano et al.*, 2006] suggests that a scenario with such large values of

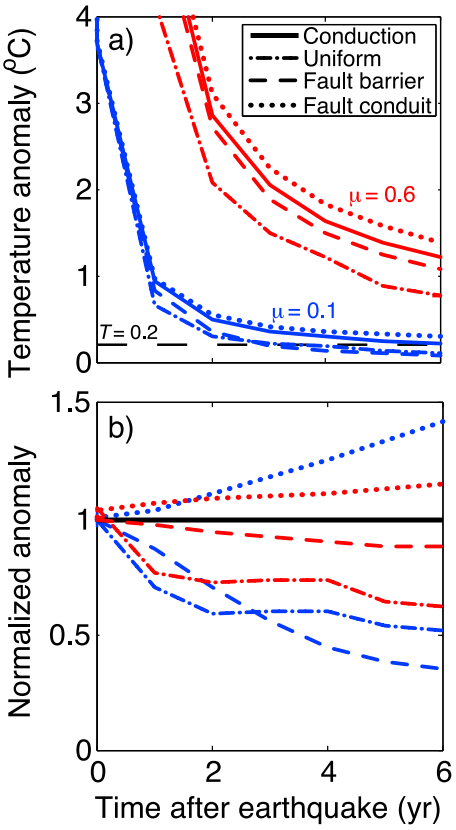

Figure 3. (a) Thermal response to frictional heating and fluid flow for a thrust fault at 2 km and for friction coefficients during slip of 0.6 (red lines) or 0.1 (blue lines). The purely conductive results are shown as solid lines for comparison. The black horizontal dashed line at 0.2°C reflects an ideal minimum target anomaly for detection. (b) The temperature anomalies normalized to the conductive scenarios as a function of time. The lines in both panels correspond to the different fault zone architectures.

fault zone permeability, which allows for large thermal disturbances from advection is probably anomalous rather than typical.

[14] In a third set of model simulations, we evaluate the effects of a low permeability fault zone (10^{-19} m^2) within high permeability country rock, as might be expected for a fine-grained or clay-rich fault core. As in the scenarios described above, significant advective disturbances appear within the first 2 years after an earthquake only if country rock permeability is ~10^{-14} m^2 or greater (Figure 2c). Temperatures within and near the fault zone behave diffusively, but upward fluid flow increases the country rock temperature and the background geotherm. Because the temperature anomalies are relative to the background geotherm, the net effect is to reduce the peak temperature anomaly (Figure 3b). For this scenario, when the background geotherm is removed slightly negative temperature anomalies bound the peak temperature anomaly (Figure 2c); this is not a result of cooling in these areas but rather indicates that the region near the fault was less affected by advection and the resulting temperature increase than the surrounding country rock. For our low-friction scenario, the anomaly is ~14% less than the conductive solution 1 year after the earthquake and ~67% less than the conductive solution after 6 years.

[15] We designed the preceding scenarios to optimize the potential for fluid flow by initializing large fluid pressures in both the fault zone and country rock. In a final set of models, we modify this initial condition to evaluate the effects of lateral fluid flow driven away from a highly pressurized fault zone, as might be expected from transient pressurization during slip [e.g., *Andrews*, 2002; *Hirose and Bystricky*, 2007] or from interseismic localization of pressure within the fault [e.g., *Rice*, 1992; *Sleep and Blanpied*, 1992; *Fulton and Saffer*, 2009b]. In these simulations, pore pressures within the fault zone and country rock are lithostatic and hydrostatic, respectively. These results (not shown) indicate that temperatures are not significantly affected by fluid flow away from the fault zone but may be affected by updip fluid flow within a high permeability fault conduit similar to the results described above.

[16] Our model results suggest that a frictional temperature anomaly is detectable at reasonable depths (~2 km) and times (up to a few years) after an earthquake, even in the presence of fluid flow resulting from large transient pore pressures and high permeabilities (Figure 3a). In all scenarios, permeabilities less than 10^{-14} m^2 yielded results that were essentially identical to those for conductive heat transfer over the time scale of a few years after an earthquake. These results differ from the case of topographically driven groundwater flow, which exhibits a smaller permeability threshold for advection ($k > \sim10^{-16}$ m^2) largely due to the fact that fluid flow is sustained for much longer periods of time, and most previous analyses assume a steady state condition [e.g., *Smith and Chapman*, 1983; *Williams and Narisimhan*, 1989; *Saffer et al.*, 2003; *Fulton et al.*, 2004]. We also find that advective disturbances to frictional heat anomalies at ~1−2 km depth are generally small immediately after an earthquake, but their relative significance increases with time (Figure 3b).

5. Borehole Temperature Measurements to Detect Frictional Heating

[17] Temperature profiles measured in boreholes intersecting fault zones shortly after large earthquakes provide the most direct opportunity for quantifying frictional heat. However, designing a borehole to detect a frictional heating anomaly with temperature profiles introduces its own set of considerations. The borehole must be drilled deep enough and fast enough so that the thermal perturbation can be detected, and once drilled, the thermal environment of the borehole must be well characterized because temperature anomalies are detected on the basis of departures from background thermal conditions. In the remainder of this study we explore other candidate processes that may mask or dissipate the frictional heating anomaly and discuss strategies for overcoming these obstacles. These processes include the thermal disturbance of drilling, variations in thermal physical rock properties such as thermal conductivity or thermal diffusivity [e.g., *Tanaka et al.*, 2007], and environmental noise within the borehole such as convection.

5.1. Thermal Disturbance From Drilling Fluids

[18] During drilling, fluids are circulated through the borehole to dissipate the mechanical heat of drilling, to stabilize

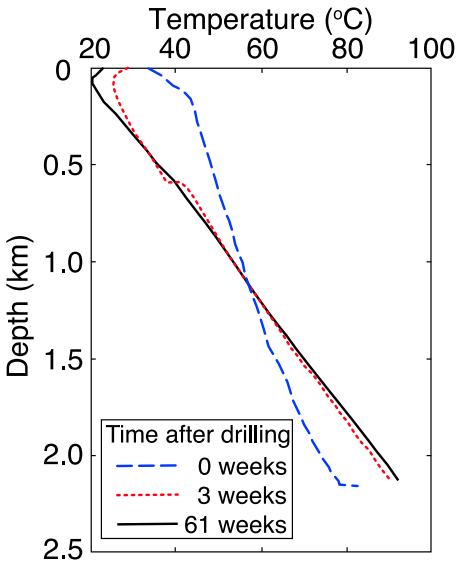

Figure 4. Temperature profiles from the SAFOD pilot hole measured after the end of drilling (blue) and measured at later times. Temperatures measured after a period of 3 weeks (red) are already close to the equilibrium temperature (black). Modified from *Williams et al.* [2004].

the borehole wall, and to transport rock cuttings out of the hole. These fluids rapidly absorb the mechanical heat of drilling but impart a thermal disturbance to the borehole wall. The fluids enter the borehole at approximately the surface temperature and rapidly travel down inside the drill pipe and then back to the surface through the borehole annulus. At the bottom of deep boreholes, drilling fluids are well below the ambient temperature absorbing heat, and in the upper part of the borehole returning fluids are above ambient temperatures releasing heat (e.g., Figure 4). During the borehole circulation period, the disturbance behaves as a line source that grows in length over time. The source strength depends on many factors, but at each depth, the disturbance is primarily a function of the temperature difference between the circulating fluid and borehole wall, and the length of time fluids are in contact with the borehole wall [*Lachenbruch and Brewer*, 1959]. As a result, the bottom of a borehole generally reequilibrates more quickly than the top because it is exposed to drilling fluids for a relatively short time. A rule of thumb suggests that following the cessation of circulation, it takes approximately 4 times the duration a borehole section is exposed to circulating fluids to reequilibrate. Borehole temperature profiles from previous fault zone drilling efforts are reported to have equilibrated to within 0.01°C within approximately 6 months after the cessation of circulation [e.g., *Williams et al.*, 2004; *Kano et al.*, 2006]. However, the nonlinear influence of a drilling disturbance on the detection of a frictional heat anomaly as a function of time has not been previously evaluated.

[19] We model the effect of borehole circulation to assess its impact on the thermal field using a cylindrical model of conductive heat transfer. The primary assumption of this modeling is that heat transfer from the borehole wall to the surrounding country rock is conductive. This assumption allows us to linearly combine the frictional heating signal with the borehole drilling disturbance and is justified because in most cases, borehole mud weight is balanced with formation pore pressure by design, specifically to limit circulation losses or fluid entry from the formation into the hole [e.g., *Zoback*, 2007]. We do not consider scenarios including the effects of serious drilling problems where large amounts of drilling fluids flood the formation. We prescribe a borehole disturbance similar to that observed within the 2.2 km San Andreas Fault Observatory at Depth (SAFOD) pilot hole [*Williams et al.*, 2004] (Figure 4). Note that a common feature with drilling disturbances, as in this example and temperature profiles from the Cajon Pass scientific research drill hole [*Sass et al.*, 1992], is an inflection point in the borehole temperature disturbance between the lower part of the hole where heat is extracted and the top part of the hole where heat is deposited. In this case, the inflection point is at ~1200 m depth. To simplify the modeling we only model the lower portion of the borehole and surrounding country rock because this interval contains the fault zone and the temperature response in the upper portion is not important for this analysis.

[20] We validate our approach to modeling the thermal disturbance of drilling by simulating the response to the drilling disturbance observed at the SAFOD pilot hole. In these simulations, frictional heating is not included. The model does, however, include thermal properties and a background geotherm based on values appropriate for the SAFOD pilot hole [*Williams et al.*, 2004]. At 2 km depth, the depth of interest for our analysis, we simulate the drilling disturbance for 4 days similar to that experienced. Temperature profiles are available after the cessation of circulation and then 3 weeks and 1 year later [*Williams et al.*, 2004]. Comparison of the simulated temperature recovery at 2 km depth is similar to that observed (not shown), suggesting that the disturbance and recovery are dominated by conduction and that our modeling approach, described below, is reasonable for evaluating the effects of drilling disturbance on the frictional heat anomaly.

[21] For our combined conductive models of the frictional heating signal and the drilling disturbance, the borehole and model domain have a radius of 0.1 m and 1 km, respectively. We assume a horizontal fault zone at 2 km depth and place the top and bottom of the model at depths of 1200 and 2200 m, respectively. The lower boundary is assigned a heat flux of 45 mW/m^2, consistent with our transient fluid flow models. The upper boundary corresponds to the inflection point noted above and prescribed with a constant temperature of 43.2°C. This temperature is based on the background geotherm and thermal properties consistent with those in our fluid flow models, including a thermal conductivity of 2.18 Wm^{-1} K^{-1} and thermal diffusivity is 1×10^{-6} m s^{-2}

[22] We use the finite difference code SHEMAT to solve for cylindrical-symmetric transient heat conduction [*Clauser*, 2003]. Model simulations are initialized with a temperature field following the background geothermal gradient superimposed with a temperature anomaly expected from frictional heating defined by equations 1 and 2 for our low-friction case at 2 km depth, 1 year after an earthquake with 5 m of slip (Figure 5a, red line). Thus, we are assuming the fault zone is intersected 1 year after the earthquake. The drilling disturbance from fluid circulation is simulated by prescribing temperatures within the borehole between the inflection point and the bottom of the borehole. The prescribed temperatures

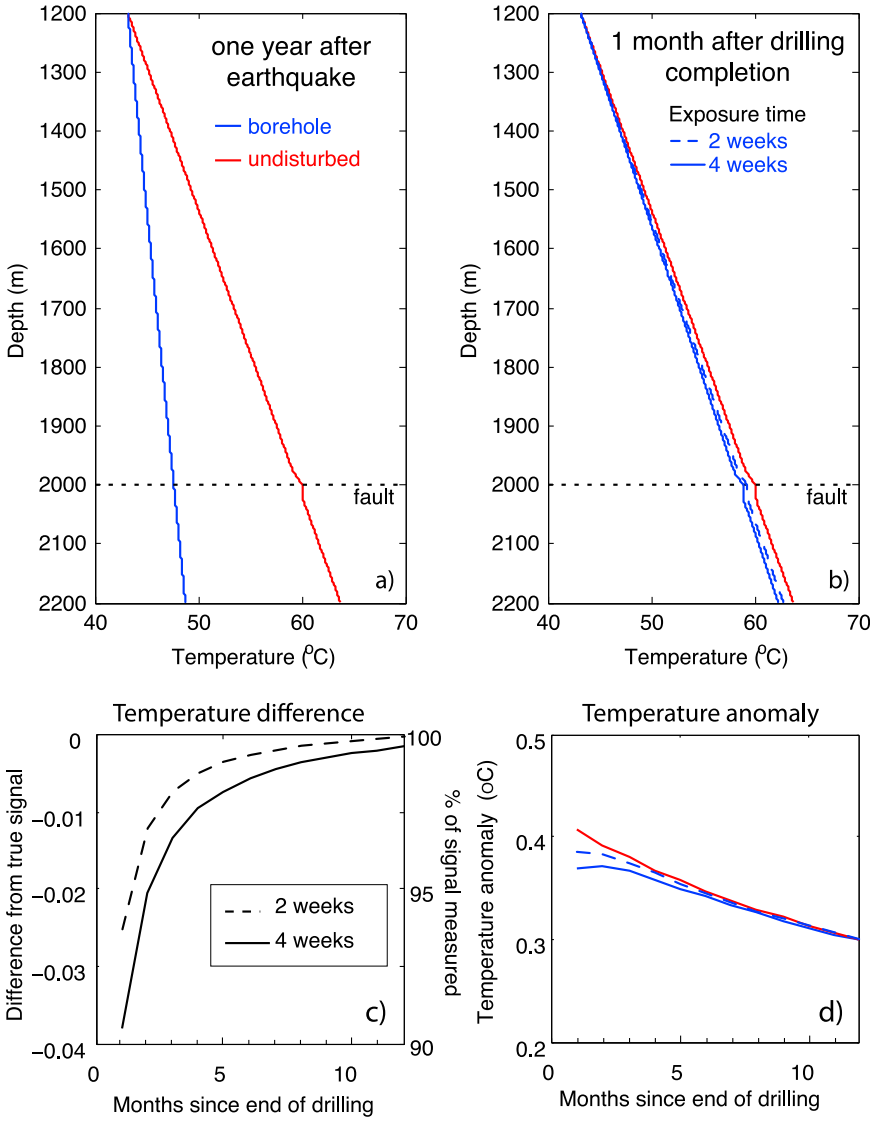

Figure 5. Results of drilling disturbance model simulations. (a) Temperature profile far from borehole 13 months after simulated earthquake with low friction coefficient assuming hydrostatic pore pressure (red line) and prescribed borehole disturbance based on SAFOD pilot hole observations (blue line). Temperatures due to the drilling disturbance are held constant for 1 month. (b) Temperature profiles 14 months after the earthquake; 1 month after the end of drilling and borehole circulation. Temperatures due to drilling disturbance held constant for 1 month (solid line) and 2 weeks (dashed line). (c) The difference between the simulated borehole anomaly and the anomaly without any drilling disturbance. (d) Temperature anomaly as a function of time after drilling in the borehole (blue) compared to profiles unaffected by drilling disturbance (red).

increase with a constant gradient from the inflection point at 1200 m to 15°C cooler than background conditions at the base of the borehole at 2200 m (Figure 5a, blue line). These values are consistent with observations within the SAFOD pilot hole (Figure 4). Frictional heat is not included in the line source initial condition. These prescribed temperatures are held constant for 4 weeks of simulation time allowing the cooling effects of fluid circulation to propagate into the surrounding rock. In our simulations, 4 weeks represents the time during which the fault zone is exposed to borehole circulation; the total time to drill the borehole following the earthquake is 1 year and 4 weeks. Four weeks likely represents the maximum time it would take to drill from 2 to 2.2 km. For the SAFOD pilot hole, this took ~4 days (SAFOD Pilot Hole daily reports: http://www.icdponline.org/contenido/icdp/front_content.php?idart=1036). Because temperatures representing the drilling disturbance are held constant rather than growing to this value over the 4 week drilling period, the source strength, and thus simulated drilling disturbance, should both be viewed as maxima. After 4 weeks the prescribed temperatures within the borehole are allowed to relax and the model progresses in time. We use a time step of 1 month. During this time, both the frictional heat anomaly and the drilling disturbance diffuse through the model domain.

For comparison, we also ran simulations corresponding to a fault zone exposure to the drilling disturbance of 2 weeks.

[23] One month after the cessation of drilling, corresponding to 1 and 2 times the amount of time the fault zone was exposed to drilling, the drilling disturbance has relaxed significantly, and after 4 times the duration of fault zone exposure (corresponding to 4 and 2 months, respectively), the drilling disturbance has largely dissipated and the frictional heat signal is similar to that expected without any disturbance (Figure 5). The rapid attenuation of the drilling disturbance is consistent with temperature observations at the SAFOD pilot hole (Figure 4) and theoretical considerations [*Lachenbruch and Brewer*, 1959; *Williams et al.*, 2004]. Even at just 1 month after drilling, the frictional heat signal in the borehole is apparent (Figure 5b), and the observed frictional heat anomaly reflects 91% of the true anomaly across the fault (Figure 5c) for simulations with 4 weeks of fault zone exposure to borehole circulation and 94% for 2 weeks of exposure (Figures 5b–5c). This signal recovery increases to 99% at 7 months and 99.5% at 1 year for the simulations with 4 weeks of disturbance and reaches 99% at 5 months and 99.9% at 11 months for the 2 week long disturbance simulations. These results suggest that the drilling disturbance does not adversely impact the resolution of a frictional heat signal given sufficient relaxation time.

5.2. Thermal Physical Rock Properties

[24] For conductive heat transfer the thermal gradient is inversely proportional to the thermal conductivity, and therefore variations in thermal conductivity have the potential to cause perturbations in the thermal gradient that might be misinterpreted as a frictional heating signal. Thermal conductivity varies with density, porosity, grain size, degree of cementation, and mineral composition [e.g., *Brigaud and Vasseur*, 1989; *Hartmann et al.*, 2005]. Low values of thermal conductivity associated with fault gouge or highly fractured rock may locally perturb temperatures and could be misinterpreted as a very small frictional heat signal [e.g., *Tanaka et al.*, 2007]. Additionally, thermal diffusivity, the ratio of the thermal conductivity to heat capacity, governs the transient response of the system to a heat source. Documenting these rock properties is particularly important within a fault zone itself, where thermal physical rock properties may vary due to the brecciation of country rock, potential hydrothermal alteration of minerals, and potential anisotropy effects due to large strain.

[25] Determination of thermal properties from core samples or rock chips can be used in conjunction with geophysical logs to help characterize the effects of heterogeneity in thermal properties [e.g., *Tanaka et al.*, 2007]. Thermal conductivity scales with thermal diffusivity and is readily measured in the lab on either hand samples or rock chips to an accuracy of ~5% [*Sass et al.*, 1971]. Other perturbations to the background thermal field, such as radiogenic heat production, topography, uplift and erosion, or subsidence and burial, produce low wave number variations that are not likely to be mistaken for the effects of frictional heating. Higher wave number variations due to heterogeneous thermal conductivity that may be mistaken for frictional heat are generally small (<~0.1°C) [e.g., *Tanaka et al.*, 2007]. If thermal conductivity does not change considerably over time, then these effects may be characterized and removed through modeling based on values determined from core analysis [e.g., *Tanaka et al.*, 2007] or with the use of repeat temperature profiles, which we describe in more detail in section 5.4.

5.3. Borehole Convection

[26] In addition to potentially high wave number thermal disturbances due to heterogeneous rock properties, convection cells within boreholes can develop and generate high wave number disturbances adding noise to the temperature measurements. Casing the borehole, plugging the bottom and filling the casing with a fluid to suppress convective heat transfer, however, can stabilize the borehole environment. The most straightforward way to suppress convection is with a high-viscosity fluid in a small diameter borehole [*Hales*, 1937; *Krige*, 1939; *Misener and Beck*, 1960]. Variations in borehole diameter outside of the casing may also contribute to convective noise because convection of fluids between the annulus and country rock may also generate thermal perturbations that distort frictional heating anomalies. Thoughtful borehole design that minimizes annular space between the borehole and the country rock and the use of designated sampling tubes separated from the surrounding borehole casing by baffles can help reduce convection and its effect on thermal measurements.

5.4. Borehole Temperature Measurements and Repeated Temperature Profiles

[27] Specific logging conditions are needed to quantify the size and shape of the temperature anomaly that may result from frictional heating. High-precision thermistors have the ability to measure temperatures to a few mK or less [e.g., *Beck and Balling*, 1988; *Clow*, 2008] and in general do not limit the signal-to-noise ratio. However, taking advantage of high-precision thermistors requires logging procedures that differ from other open-hole logs in several respects. First, although most borehole logs are collected from the bottom of the borehole upward, precision temperature profiles must be measured on the way down so that the logging tool does not disturb the measuring environment. Second, most logging tools are moved at a constant rate during logging. In contrast, measuring temperatures at a constant rate requires precisely deconvolving the instrument response from the signal. Third, if temperatures are being recorded at the surface, eliminating slip ring noise may also require additional filtering [e.g., *Saltus and Clow*, 1994]. An alternative approach is to stop the instrument at specific depth intervals, typically 1 m or less, for ~60 s or so to allow the thermistor to approach equilibrium (i.e., a "stop-go" technique). This measurement time is typically several times the time constant for most temperature probes, which allows for more accurate extrapolation to true formation temperature [*Harris and Chapman*, 2007]. Finally, precision temperature profiles need to be measured in a stable borehole environment and thus it is necessary to allow for temperatures to restabilize after drilling and other logging procedures. These considerations often necessitate dedicated logging trips, but can provide high precision data that effectively characterizes the subsurface temperature field.

[28] Repeated temperature profiles on a monthly to annual time scale provide a number of tools for understanding and analyzing the thermal regime that are unavailable with a single temperature profile. Many background disturbances within the borehole can be removed and the effects of tran-

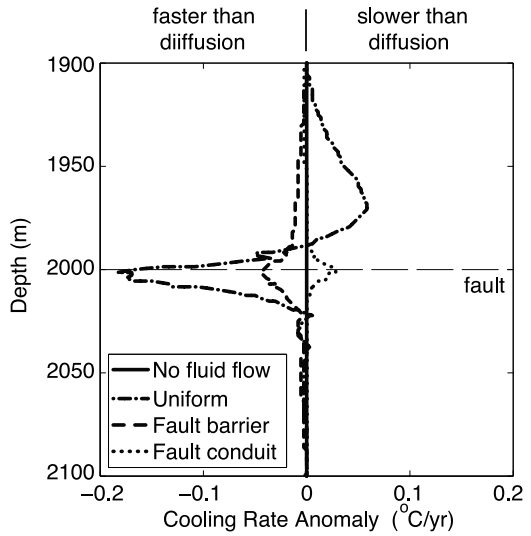

Figure 6. Cooling rates relative to purely diffusive heat transfer between years 1 and 2 for advective scenarios that include permeabilities of 10^{-14} m^2. Curves show areas where the model results from 2 years after an earthquake diffused faster or slower than expected by forward projecting (i.e., conductively cooling) the simulated borehole temperatures extracted for the same scenario 1 year after an earthquake. Cooling rate anomalies show where heat has been extracted (negative anomalies) or deposited (positive) by advection during the time between logs.

sient groundwater flow or frictional heat generation may be characterized with the use of repeated temperature profiles. This technique is especially valuable in distinguishing the effects of temperature perturbations due to heterogeneous rock properties that are steady state from transient thermal perturbations [e.g., *Chapman and Harris*, 1993; *Yamano and Goto*, 2001]. Steady state thermal disturbances that might be mistaken for a frictional heat anomaly or that disturb frictional heat anomalies can be investigated and removed by differencing repeated profiles [*Chapman and Harris*, 1993; *Davis et al.*, 2010]. Additionally, borehole temperature profiles measured at earlier times can be diffused forward in time and compared with later profiles [*Carslaw and Jaeger*, 1959]. This technique provides a way of estimating thermal diffusivity and evaluating whether perturbations are constant in time or changing at a rate inconsistent with thermal diffusion. These determinations can be used to support interpretation of heterogeneities in rock properties (constant in time), fluid flow (likely changing inconsistent with thermal diffusion), or frictional heat (diffusing with time).

[29] We illustrate the utility of repeated temperature profiles for aiding interpretations of diffusive and advective heat transfer. Here we use our simulation of the combined effects of frictional heat generation and fluid flow computed 1 year (profile 1) and 2 years (profile 2) after the earthquake. For this discussion we assume that drilling disturbances have attenuated and that thermal physical rock properties are constant with depth. We diffuse profile 1 one year forward in time assuming purely diffusive heat transfer and subtract this forward continued profile from profile 2. The difference between these two profiles reflects the influence of fluid flow between years 1 and 2. This difference is the cooling rate relative to diffusion for the period between profiles. For each fault zone architecture, the difference between the forward projection of profile 1 and profile 2 reveal distinctly different cooling rate patterns due to the effects of fluid flow (Figure 6). The uniform permeability scenario cools more quickly below the fault zone and more slowly immediately above the fault zone than predicted by diffusion alone. This result is consistent with fluids moving upward and spreading the anomaly as discussed in section 4. In contrast, the fault barrier architecture scenario cools more slowly than conduction both above and below the fault. In the fault conduit scenarios, fluid flow along the fault plane increases fault zone temperatures and the frictional heat anomaly dissipates more slowly than predicted. Additionally, in this scenario, the peak temperature anomaly is displaced upward. These results show that repeated temperature profiles can not only help discriminate between diffusive and advective heat transfer but may also provide insight into the hydrogeology and may allow precise estimates of frictional heating to be made in the presence of advection. Multiple sets of repeated temperature profiles yield greater insight into the nature of heat transfer within the fault zone and offer the potential of additionally identifying vertical variations in thermal physical rock properties. We note, however, that in natural systems, the interpretation of repeated temperature logs may be more complex than described here, particularly if physical properties change as fractures heal over time after an earthquake. Downhole monitoring of other geophysical properties (e.g., seismic velocity) may help in assessing these changes. We conclude that it would be beneficial to collect temperature profiles on a regular basis as long as a signal exists.

6. Comparison With Data

[30] Attempts to estimate the frictional heat generation of large earthquakes (1995 M_w 6.9 Kobe, Japan; 1999 M_w 7.6 Chi-Chi, Taiwan) with temperature profiles have previously been carried out [*Yamano and Goto*, 2001; *Kano et al.*, 2006; *Tanaka et al.*, 2006, 2007], and drilling across the Wenchuan Fault in response to the 2008 M_w 7.9 Sichuan earthquake in China is currently underway. These fault zone drilling experiments provide a wealth of important information regarding earthquake processes [e.g., *Yamano and Goto*, 2001; *Tanaka et al.*, 2001, 2006; *Ma et al.*, 2006; *Kano et al.*, 2006].

[31] Temperatures at Chelungpu were measured 15 months after the 1999 Chi-Chi earthquake in Taiwan (M_w = 7.6) in a shallow borehole that intersected the fault at ~300 m depth and then 6 years after the earthquake in a deeper borehole crossing the fault at 1111 m depth [*Kano et al.*, 2006; *Tanaka et al.*, 2006]. Temperatures were measured 3 weeks and 7 months after circulation stopped in the shallow and deep borehole, respectively. Continuous temperature measurements made at a fixed depth of about 1 km in the more extensively characterized deep hole indicate that the drilling disturbance had reequilibrated.

[32] Temperature measurements at Chelungpu document a small anomaly of ~0.12°C at ~300 m depth in the shallow hole 15 months after the earthquake and an anomaly of 0.06°C at 1111 m depth 6 years after the earthquake. These small anomalies are interpreted to reflect low frictional resistance during slip (friction coefficient of ~0.1 assuming

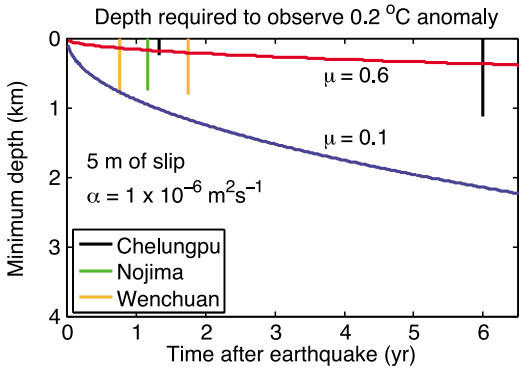

Figure 7. Curves show the minimum depth a borehole must intersect the fault zone to observe a temperature anomaly of 0.2°C as a function of time, for friction coefficients of 0.6 (red lines) and 0.1 (blue lines) assuming hydrostatic pore pressure, and assuming conduction-dominated heat transfer and a thrust earthquake with 5 m of slip. For reference, the depth and timing of completion of rapid response fault drilling experiments to date are shown as vertical lines at the top of the panel, although their respective parameters may be different than modeled here. The holes for Wenchuan reflect anticipated depth and timing.

hydrostatic pore pressure), but ambiguity concerning whether the anomaly is affected by transient fluid flow or heterogeneous thermal properties remains [*Kano et al.*, 2006; *Tanaka et al.*, 2006, 2007]. Our transient fluid flow models illustrate that peak temperature anomaly values 6 years after an earthquake are scaled by a factor of ~0.4–1.4, depending on the exact permeability architecture. At the depth of the deep temperature measurements (1111 m), the fault is interpreted to have a ~1 m thick damage zone with permeabilities of 10^{-16} m^2 or less within lower permeability country rock [*Doan et al.*, 2006]. Our models suggest that temperatures would not be affected by advection for these permeabilities. With a wider damage zone acting as a permeable conduit (10 m), our results suggest that the temperature anomaly would be increased by as much as ~0.09°C 6 years after an earthquake in a scenario with fault zone permeability 2 orders of magnitude greater than determined for the Chelungpu fault at depth. This increase in temperature corresponds to an anomaly ~40% above the conductive solution (Figure 3b) and would result in slight overestimates of the frictional resistance during slip rather than an underestimate of frictional resistance. The thermal anomaly across the Chelungpu fault has been variously interpreted in terms of frictional heating [*Kano et al.*, 2006] or heterogenous rock properties [*Tanaka et al.*, 2007], although the latter interpretation has been questioned [*Kano et al.* 2007]. Unfortunately, deteriorating hole conditions prevented the ability to repeat temperature profiles. However, in either case, our results suggest that the inferences of low friction during slip based on either a small thermal perturbation or lack of a thermal perturbation are robust.

[33] Temperature measurements were also made within a borehole that intersected the Nojima fault at 624 m depth 2.5 years after the 1995 M_w 6.9 Kobe, Japan, earthquake [*Yamano and Goto*, 2001]. However, because the primary purpose of these measurements was to measure background heat flux and monitor groundwater flow, fiber-optic-based distributed temperature sensing was used for the measurements, which provided high spatial and temporal resolution but was unable to discriminate temperature anomalies <0.3°C and did not reveal a frictional heat signal. These data are also consistent with inferences of low friction during slip.

7. Discussion

[34] There has been a growing interest in drilling across fault zones after large earthquakes. Rapid response boreholes can allow the direct observation of temperature anomalies generated by frictional heating and characterization of other in situ properties relevant to understanding faulting processes [e.g., *Tanaka et al.*, 2001; *Ma et al.*, 2006; *Brodsky et al.*, 2009]. The combination of these observations can potentially shed light on reasons the friction coefficient during slip is or appears to be so low. Future drilling projects will yield even greater insight into variations of friction and its dependency on slip, geometry, and fault history if they are designed to be sensitive to the hydrogeological constraints and low values of friction.

[35] We estimate that a conservative limit for the unambiguous detection and interpretation of a frictional heat anomaly is ~0.2°C. This magnitude is well above the detectable limits of borehole temperature measurements and is likely distinguishable from the effects of borehole convection and subsurface heterogeneity in thermal physical properties. Figure 7 illustrates the trade-offs between drilling depth and time for both of our high-friction and low-friction cases. The minimum depth along the fault where a temperature anomaly of at least 0.2°C is expected after a thrust earthquake with 5 m of slip is shown as a function of time. Two years after an earthquake, a borehole would need to intersect the fault at 1.24 km depth for a weak fault with μ = 0.1, whereas after 6 years, the minimum depth would need to be 2.14 km. These estimates are based on conductive heat transfer alone. Our fluid flow model results suggest conductive heat transfer is a reasonable approximation for the first few years after an earthquake, even for the most advectively disturbed cases, we explored (Figure 3). Superimposed on Figure 7 are the depth extent and timing of previous and ongoing rapid response fault zone drilling experiments. Although the parameters for these particular earthquakes may be different than modeled here, our results suggest that, in general, boreholes less than ~1 km deep may not be deep enough to capture a substantially large thermal anomaly from a fault with very low frictional resistance during slip. The trade-offs between borehole depth and time emphasize that drilling costs can be decreased if drilling can be mobilized very quickly because the necessary depth to observe a substantial frictional heat anomaly can be reduced.

[36] We realize that the detection of substantial thermal anomalies from frictional heating will not answer all our questions regarding the frictional behavior of faults. The residual temperature on a fault some time after slip (several times longer than the duration of the slip event) is a result of the integrated heat production during slip, and thus, measurements of residual heat on faults can only resolve the average friction coefficient during slip. Although thermal measurements may not be able to resolve the temporal evolution of frictional heat generation and dynamic friction, the displacement averaged value of friction does provide insight

into whether friction reached very low values during slip and is possibly the most clear in situ measure of fault friction during earthquake slip.

[37] In this study, we addressed three specific questions regarding the effects of transient fluid flow on the frictional heat signal from an earthquake: (1) how big is the expected fault zone temperature anomaly as a function of time? (2) under what conditions might transient groundwater flow disturb the frictional heat signal? (3) how does advection affect the frictional heat signal for different fault zone permeability architectures? Our modeling suggests that a frictional heat anomaly of at least 0.2°C, associated with a thrust earthquake having an effective coefficient of friction of 0.1 and ~5 m of slip or greater, is resolvable for approximately 4 years or more in a 2 km borehole. In addition, we find that the effects of transient groundwater flow on the frictional heat signature after an earthquake are likely only significant when permeabilities have high values $>\sim 10^{-14}$ m^2. Our results also illustrate that when the fault zone acts as a permeable conduit within lower permeability country rock, as at the Chelungpu Fault, the effects of transient groundwater flow would, at most, increase the fault zone temperature anomaly rather than mask it. The potential for increasing temperatures due to transient hydrological circulation has not been described in previous work and is novel to this work. We also find that the thermal disturbances of fluid circulation during drilling do not present insurmountable problems to capturing a frictional heating signal. Taken together, these results suggest that if the frictional strength of Chelungpu were high, a much larger temperature perturbation would have been observed. The lack of a significantly large observed frictional heating signal implies that the frictional strength of Chelungpu is low. Our results show that a borehole drilled rapidly after a large earthquake holds the promise of unequivocally providing an in situ measure of fault strength.

8. Conclusions

[38] Our study of the frictional heating across fault zones allows the following conclusions to be made:

[39] 1. Numerical simulations for a range of realistic permeability, frictional heating, and pore pressure scenarios show that transient fluid flow associated with an earthquake is unlikely to significantly perturb the frictional heat signal within a few years after an earthquake unless the permeability is high ($>\sim 10^{-14}$ m^2).

[40] 2. Thermal perturbations resulting from the circulation of fluids during drilling diffuse much more rapidly than the frictional heating signal and do not present a large impediment to determining fault strength from borehole temperature profiles.

[41] 3. Repeated temperature profiles can aid in identifying and removing steady state and transient disturbances to the subsurface temperature field and provide a greater degree of confidence in identifying borehole temperature perturbations from frictional heating. Borehole design and attention to measuring techniques can improve the signal-to-noise ratio.

[42] 4. Accessing the heat anomaly quickly maximizes the likelihood of unambiguously detecting a frictional heat signal. The frictional heat anomaly diminishes with the square root of time while the relative disturbance from transient fluid flow, if any, increases.

[43] These results suggest that models of conductive heat transfer can be used to design boreholes where the objective is to measure the frictional heat generation of earthquakes. Drilling to 1 km depth within a year of an earthquake or 2 km depth within 2 years should allow unambiguous detection of thermal anomalies from frictional heating.

Appendix A

[44] For our coupled fluid flow and heat transport modeling, we use the finite-element algorithm SUTRA to solve the governing equations of conservation of mass and energy. For our model simulations, the fluid mass balance is defined by *Voss* [1984];

$$\rho_f(\phi\beta_f + (1-\phi)\beta_s)\frac{\partial P}{\partial t} + \left(\phi\frac{\partial P}{\partial T}\right)\frac{\partial T}{\partial t} - \nabla\left[\left(\frac{k\rho_f}{\eta}\right)(\nabla P - \rho_f g)\right] = 0, \quad \text{(A1)}$$

where ϕ is porosity, β_f (Pa^{-1}) and β_s (Pa^{-1}) are fluid and matrix compressibility, η is fluid viscosity (Pa-s) and is a function of temperature, P is pressure (Pa), T (°C) is fluid temperature, k is the permeability tensor (m^2), and g is gravity (m-s^{-2}). ρ_f is the fluid density of water, which is a function of temperature with a value of 1000 kg/m^3 at 20°C and a coefficient of fluid density change per degree of temperature change of −0.375 kg-m^{-3} K^{-1}.

[45] The solid matrix-fluid energy balance is defined by *Voss* [1984]:

$$\frac{\partial}{\partial t}[\phi\rho_f c_f + (1-\phi)\rho_s c_s]T + \nabla(\phi\rho_f c_f v_f T) - \nabla([\lambda_f + (1-\phi)\lambda_s]I + \phi\rho_f c_f D)\nabla T = (1-\phi)\rho_s\gamma_s, \quad \text{(A2)}$$

where c_f (J kg^{-1}K^{-1}) and c_s (J kg^{-1}K^{-1}) are fluid and matrix specific heat, v_f (m-s^{-1}) is the average fluid velocity, λ_f (Wm^{-1} K^{-1}) and λ_s (Wm^{-1} K^{-1}) are the fluid and matrix thermal conductivity, D (m) is the dispersivity tensor that accounts for the contribution of energy transport due to irregular fluid flow and is prescribed latitudinal and longitudinal values of 0.5 m. γ_s (J kg^{-1}s^{-1}) is the solid matrix heat source, which may consist of either radioactive heat production or frictional heat generation. Further details regarding SUTRA are described in the study by *Voss* [1984].

[46] For our models that simulate the thermal recovery from drilling disturbances (section 5.1), we use the finite-difference code SHEMAT [*Clauser*, 2003] to solve for cylindrical-symmetric transient heat conduction. The governing equation for this analysis is based on the conservation of energy and defined by:

$$\frac{\partial}{\partial t}[\phi\rho_f c_f + (1-\phi)\rho_s c_s]T - \frac{1}{r}\frac{\partial}{\partial r}\left([\lambda_f + (1-\phi)\lambda_s]r\frac{\partial T}{\partial r}\right) - \frac{1}{r^2}\frac{\partial}{\partial\varphi}\left([\lambda_f + (1-\phi)\lambda_s]\frac{\partial T}{\partial\varphi}\right) - \frac{\partial}{\partial z}\left([\lambda_f + (1-\phi)\lambda_s]\frac{\partial T}{\partial z}\right) = (1-\phi)\rho_s\gamma_s, \quad \text{(A3)}$$

where r is the radial direction away from the center, φ is the azimuthal direction, and z is the depth direction.

[47] **Acknowledgments.** We thank C. Williams for providing SAFOD temperature logs used in Figure 4 and N. de Paola and an anonymous reviewer and Associate Editor for constructive comments and reviews that have helped improve this manuscript. This project was supported by NSF grants EAR 0746192 and EAR 0125189 to Saffer and EAR 0545342 to Harris.

References

Andrews, D. J. (2002), A fault constitutive relation accounting for thermal pressurization of pore fluid, *J. Geophys. Res.*, *107*(B12), 2363, doi:10.1029/2002JB001942.

Beck, A. E., and N. Balling (1988), Determination of virgin rock temperatures, in *Handbook of Terrestrial Heat Flow Density Determination*, 1st ed., edited by R. Haenel, L. Rybach, and L. Stegena, pp. 59–85, Kluwer Acad., Boston, Mass.

Brigaud, F., and G. Vasseur (1989), Mineralogy, porosity, and fluid control on thermal conductivity of sedimentary rocks, *Geophys. J. Int.*, *98*, 525–542.

Brodsky, E. E., and H. Kanamori (2001), Elastohydrodynamic lubrication of faults, *J. Geophys. Res.*, *106*, 16,357–16,374, doi:10.1029/2001JB000430.

Brodsky, E. E., et al. (2009), Rapid response fault drilling: Past, present, and future, *Sci. Drill.*, *8*, 66–74, doi:10.2204/iodp.sd.8.11.2009.

Brune, J. N., T. L. Henyey, and R. F. Roy (1969), Heat flow, stress, and rate of slip along the San Andreas Fault, California, *J. Geophys. Res.*, *74*(15), 3821–3827.

Byerlee, J. D. (1978), Friction of rocks, *Pure Appl. Geophys.*, *116*, 615–626.

Carslaw, H. S., and J. C. Jaeger (1959), *Conduction of Heat in Solids*, Clarendon, Oxford, U. K.

Chapman, D. S., and R. N. Harris (1993), Repeat temperature measurements in borehole GC-1, northwestern Utah: Towards isolating a climate-change signal in borehole temperature profiles, *Geophys. Res. Letts.*, *18*, 1891–1894.

Clauser, C., (ed.) (2003), *Numerical Simulation of Reactive Flow in Hot Aquifers*, Springer, New York.

Clow, G. D. (2008), USGS polar temperature logging system, description and measurement uncertainties, *U.S. Geol. Surv. Tech. Methods*, *2–E3*, 24 pp.

Davis, M. G., R. N. Harris, and D. S. Chapman (2010), Repeat temperature measurements in boreholes from northwestern Utah link ground and air temperature changes at the decadal time scale, *J. Geophys. Res.*, *115*, B05203, doi:10.1029/2009JB006875.

Di Toro, G., D. L. Goldsby, and T. E. Tullis (2004), Friction falls towards zero in quartz rock as slip velocity approaches seismic rates, *Nature*, *427*, 436–439.

Doan, M. L., E. E. Brodsky, Y. Kano, and K. F. Ma (2006), In situ measurement of the hydraulic diffusivity of the active Chelungpu Fault, Taiwan, *Geophys. Res. Lett.*, *33*, L16317, doi:10.1029/2006GL026889.

Fulton, P. M., and D. M. Saffer (2009a), Effect of thermal refraction on heat flow near the San Andreas Fault, Parkfield, California, *J. Geophys. Res.*, *114*, B06408, doi:10.1029/2008JB005796.

Fulton, P. M., and D. M. Saffer (2009b), Potential role of mantle-derived fluids in weakening the San Andreas Fault, *J. Geophys. Res.*, *114*, B07408, doi:10.1029/2008JB006087.

Fulton, P. M., D. M. Saffer, R. N. Harris, and B. A. Bekins (2004), Re-evaluation of heat flow data near Parkfield, CA: Evidence for a weak San Andreas Fault, *Geophys. Res. Lett.*, *31*, L15S15, doi: 10.1029/2003GL019378.

Ge, S., and G. Garven (1992), Hydromechanical modeling of tectonically driven groundwater flow with application to the Arkoma Foreland Basin, *J. Geophys. Res.*, *97*, 9119–9144.

Hales, A. L. (1937), Convection currents in geysers, *Mon. Not. R. Astron. Soc., Geophys. Suppl.*, *4*, 122–131.

Harris, R. N., and D. S. Chapman (2007), Stop-go temperature logging for precision applications, *Geophysics*, *72*, 119–123

Hartmann, A., V. Rath, and C. Clauser (2005), Thermal conductivity from core and well log data, *Int. J. Rock Mech. Min. Sci.*, *42*, 1042–1055.

Hirose, T., and M. Bystricky (2007), Extreme dynamic weakening of faults during dehydration by coseismic shear heating, *Geophys. Res. Lett.*, *34*, L14311, doi:10.1029/2007GL030049.

Kano, Y., J. Mori, R. Fujio, H. Ito, T. Yanagidani, S. Nakao, and K.-F. Ma (2006), Heat signature on the Chelungpu fault associated with the 1999 Chi-Chi, Taiwan earthquake, *Geophys. Res. Lett.*, *33*, L14306, doi:10.1029/2006GL026733.

Kano, Y., J. Mori, R. Fujio, T. Yanagidani, S. Nakao, H. Ito, O. Matsubayashi, and K.-F. Ma (2007), Precise temperature measurements and earthquake heat associated with the 1999 Chi-Chi, Taiwan earthquake, *Sci. Drill., Spec. Issue 1*, 94–96, doi:10.2204/iodp.sd.s01.40.2007.

Krige, L. J. (1939), Borehole temperatures in the Transvaal and Orange Free State, *Proc. R. Soc. London, Ser. A*, *173*(955), 450–474.

Lachenbruch, A. H., and M. C. Brewer (1959), Dissipation of the temperature effect of drilling a well in Arctic Alaska, *U.S. Geol. Surv. Bull.*, *1083*, 73–109.

Lachenbruch, A. H., and A. McGarr (1990), Stress and heat flow, in *The San Andreas Fault System, California*, edited by R. E. Wallace, *U.S. Geol. Surv. Prof. Pap.*, *1515*, 261–277.

Lachenbruch, A. H., and J. H. Sass (1980), Heat flow and energetics of the San Andreas Fault zone, *J. Geophys. Res.*, *85*, 6185–6222.

Ma, K.-F., J. Mori, S.-J. Lee, and S. B. Yu (2001), Spatial and temporal distribution of slip for the 1999 Chi-Chi, Taiwan earthquake, *Bull. Seismol. Soc. Am.*, *91*, 1069–1087.

Ma, K. F., et al. (2006), Slip zone and energetics of a large earthquake from the Taiwan Chelungpu-fault Drilling Project, *Nature*, *444*, 473–476.

Miller, S. A., C. Collettini, L. Chiaraluce, M. Cocco, M. Barchi, and B. J. P. Kaus (2004), Aftershocks driven by a high-pressure CO_2 source at depth, *Nature*, *427*, 724–727.

Misener, A. D., and A. E. Beck (1960). The measurement of heat flow over land, in *Methods and Techniques in Geophysics*, pp. 11–61, edited by S. K. Runcorn, Interscience, New York.

Mizoguchi, K., H. Takehiro, T. Shimamoto, and E. Fukuyama (2008), Internal structure and permeability of the Nojima fault, southwest Japan, *J. Struct. Geol.*, *30*, 513–524, doi:10.1016/j.jsg.2007.12.002.

Neuzil, C. E. (1986), Groundwater flow in low-permeability environments, *Water Resour. Res.*, *22*, 1163–1195.

Noir, J., E. Jacques, S. Bekri, P. M. Adler, P. Tapponnier, and G. C. P. King (1997), Fluid flow triggered migration of events in the 1989 Dobi earthquake sequence of Central Afar, *Geophys. Res. Lett.*, *24*, 2335–2338.

Rice, J. R. (1992), Fault stress states, pore pressure distributions, and the weakness of the San Andreas Fault, in *Fault Mechanics and Transport Properties of Rocks*, edited by B. Evans and T.-F. Wong, pp. 475–503, Academic, San Diego, Calif.

Rice, J. R. (2006), Heating and weakening of faults during earthquake slip, *J. Geophys. Res.*, *111*, B05311, doi:10.1029/2005JB004006.

Saffer, D. M., B. A. Bekins, and S. Hickman (2003), Topographically driven groundwater flow and the San Andreas heat flow paradox revisited, *J. Geophys. Res.*, *108*(B5), 2274, doi:10.1029/2002JB001849.

Saltus, R. W., and G. D. Clow (1994), Deconvolution of continuous borehole temperature logs: Example from the Greenland GISP2 ice core hole, *U. S. Geol. Surv. Open File Rep., OF 94-0254.*

Sass, J., A. Lachenbruch, and R. Munroe (1971), Thermal conductivity of rocks from measurements on fragments and its application to heat-flow determinations, *J. Geophys. Res.*, *76*, 3391–3401.

Sass, J. H., A. H. Lachenbruch, T. H. Moses Jr., and P. Morgan (1992), Heat flow from a scientific research well at Cajon Pass, California, *J. Geophys. Res.*, *97*(B4), 5017–5030.

Scholz, C. H. (2002), *The Mechanics of Earthquakes and Faulting*, 2nd ed., 471 pp., Cambridge Univ. Press, Cambridge, U. K.

Scholz, C. H. (2006), The strength of the San Andreas Fault: A critical analysis, in *Earthquakes: Radiated Energy and the Physics of Faulting, Geophys. Monogr. Ser.*, vol. 170, edited by R. Abercrombie et al., pp. 301–312, AGU, Washington, D. C.

Segall, P., and J. R. Rice (2006), Does shear heating of pore fluid contribute to earthquake nucleation?, *J. Geophys. Res.*, *111*, B09316, doi:10.1029/2005JB004129.

Sleep, N. H., and M. L. Blanpied (1992), Creep, compaction and the weak rheology of major faults, *Nature*, *359*, 687–692.

Smith, L., and D. S. Chapman (1983), On the thermal effects of groundwater flow: 1. Regional scale systems, *J. Geophys. Res.*, *88*(B1), 593–608.

Talwani, P., L. Chen, and K. Gahalaut (2007), Seismogenic permeability, k_s, *J. Geophys. Res.*, *112*, B07309, doi:10.1029/2006JB004665.

Tanaka, H., K. Fujimoto, T. Ohtani, and H. Ito (2001), Structural and chemical characterization of shear zones in the freshly activated Nojima fault, Awaji Island, southwest Japan, *J. Geophys. Res.*, *106*(B5), 8789–8810.

Tanaka, H., W. M. Chen, C. Y. Wang, K. F. Ma, N. Urata, J. Mori, and M. Ando (2006), Frictional heat from faulting of the 1999 Chi-Chi, Taiwan, earthquake, *Geophys. Res. Lett.*, *33*, L16316, doi:10.1029/2006GL026673.

Tanaka, H., W. M. Chen, K. Kawabata, and N. Urata (2007), Thermal properties across the Chelungpu fault zone and evaluations of positive thermal anomaly on the slip zones: Are these residuals of heat from faulting?, *Geophys. Res. Lett.*, *34*, L01309, doi:10.1029/2006GL028153.

Tanikawa, W., and T. Shimamoto (2009), Frictional and transport properties of the Chelungpu fault from shallow borehole data and their correlation with seismic behavior during the 1999 Chi-Chi earthquake, *J. Geophys. Res.*, *114*, B01402, doi:10.1029/2008JB005750. (Correction, *J. Geophys. Res.*, *114*, B05401, doi:10.1029/2009JB006461, 2009.)

Townend, J., and M. D. Zoback (2000), How faulting keeps the crust strong, *Geology*, *28*, 399–402, doi:10.1130/0091-7613(2000)28<399:HFKTCS>2.0.CO;2.

Townend, J., and M. D. Zoback (2004), Regional tectonic stress near the San Andreas Fault in central and southern California, *Geophys. Res. Lett.*, *31*, L15S11, doi:10.1029/2003GL018918.

Voss, C. I. (1984), A finite-element simulation model for saturated-unsaturated fluid density-dependent groundwater flow with energy transport or chemically reactive single-species solute transport, *U.S. Geol. Surv. Water Resour. Invest., 84-4369*.

Wang, K., T. Mulder, G. C. Rogers, and R. D. Hyndman (1995), Case for very low coupling stress on the Cascadia subduction fault, *J. Geophys. Res.*, *100*(B7), 12,907–12,918.

Williams, C. F., and T. N. Narisimhan (1989), Hydrogeologic constraints on heat flow along the San Andreas Fault: A testing of hypotheses, *Earth Planet. Sci. Lett.*, *92*, 131–143.

Williams, C. F., F. V. Grubb, and S. P. Galanis Jr. (2004), Heat flow in the SAFOD pilot hole and implications for the strength of the San Andreas Fault, *Geophys. Res. Lett.*, *31*, L15S14, doi:10.1029/2003GL019352.

Yamano, M., and S. Goto (2001), Long-term temperature monitoring in a borehole drilled into the Nojima Fault, south-west Japan, *Island Arc*, *10*, 326–35.

Yue, L.-F., J. Suppe, and J.-H. Hung (2005), Structural geology of a classic thrust belt earthquake: The 1999 Chi-Chi earthquake Taiwan (M_w 7.6), *J. Struct. Geol.*, *27*, 2058–2083, doi:10.1016/j.jsg.2005.05.020.

Zoback, M. D. (2007), *Reservoir Geomechanics: Earth Stress and Rock Mechanics Applied to Exploration, Production, and Wellbore Stability*, 449 pp., Cambridge Univ. Press, Cambridge, U. K.

E. E. Brodsky, Department of Earth and Planetary Sciences, University of California, Santa Cruz, CA 95064, USA.

P. M. Fulton and R. N. Harris, College of Oceanic and Atmospheric Sciences, Oregon State University, Corvallis, OR 97331, USA. (pfulton@coas.oregonstate.edu)

D. M. Saffer, Department of Geosciences, Pennsylvania State University, University Park, PA 16802, USA.